

Modelling the Dynamics of a Probe in vicinity of EROSS-433 with a Fourth-Order Polynomial Density Profile

El haj El ourabi^{1*} and Mohamed Bennai²

^{1*}Quantum Physics and Magnetism Team LPMC, Faculty of Science Ben M'sik, Hassan II University, Bd Commandant Driss Al Harti, Casablanca, 20670, Morocco.

²Quantum Physics and Magnetism Team LPMC, Faculty of Science Ben M'sik, Hassan II University, Bd Commandant Driss Al Harti, Casablanca, 20670, Morocco.

***Corresponding author:** El haj El ourabi, Quantum Physics and Magnetism Team LPMC, Faculty of Science Ben M'sik, Hassan II University, Bd Commandant Driss Al Harti, Casablanca, 20670, Morocco, E-mail: elourabis8@gmail.com

Received date: 18-July-2023, Manuscript No. tspa-23-106751; **Editor assigned:** 20-July-2023, Pre-QC No. tspa-23-106751 (PQ); **Reviewed:** 03-August-2023, QC No. tspa-23-106751 (Q); **Revised:** 08-August-2023, Manuscript No. tspa-23-106751 (R); **Published:** 31-August-2023, DOI. 10.37532/2320-6756.2023.11(8).366

Abstract

In the present work, we study the motion of a probe in the gravitational field generated by an elongated geo-cruiser asteroid of irregular shape, which we model by an inhomogeneous mass distribution. We propose a model of inhomogeneous mass distribution with a symmetric polynomial density profile of order 4 and then establish the analytical expression of the gravitational potential generated by this segment. The Lagrangian formalism allowed us to establish the dynamic equations of motion of the probe in the gravitational field generated by this body, which we solved numerically.

Keywords: Potential; Gravitational; Asteroids; Inhomogenous; Distribution; Geocruiser

Introduction

The study of near-Earth asteroids is of great scientific interest because of the impact and potential dangers that these celestial objects represent for our planet. Their collisions with the Earth have occurred throughout the history of our planet and have had profound effects on the biosphere. The NEAR Shomaker (1996) and Hayabusa (2003) missions landed on asteroids and provided invaluable information on their composition. The launch of Osiris-Rex (2016) aimed to collect soil samples from the geo-cruiser asteroid Benou (2020) and the capsule is scheduled to return to Earth in September 2023. The DART (Double Asteroid Redirection Test) mission (2022) succeeded in hitting and deflecting the trajectory of the Dimorphos geo-cruiser asteroid with a kinetic impactor. The asteroid belt has a large concentration of rocky and metallic objects and the dynamics in the vicinity of these small celestial objects requires the calculation of the gravitational potential. Among these objects are those with an elongated shape and the modelling of these by a linear mass distribution has generated several attempts. Riaguas A, Elipe A and Lara M calculated the potential generated by a homogeneous segment [1]. Elipe A and Lara M were interested in the dynamic study in the vicinity of the asteroid Eros-433 by exploiting the results of [2,3,1]. Some works have modelled the asteroid Castilia-4769 by a harmonic

Citation: El Elourabi H, Bennai M. Modelling the Dynamics of a Probe in vicinity of EROSS-433 with a Fourth-Order Polynomial Density Profile. J. Phys. Astron.2023;11(8):366.

polyhedron and while others have chosen an ellipsoidal model [4-7]. We have proposed a non-homogeneous model for Eros-433 whose density has a quadratic form, and we have treated the case of an anisotropic ring [8-10]. Other studies have focused on the search for periodic orbits and on the study of liberation points in the vicinity of a rotating segment [11, 12]. Studies have been carried out on a model dealing with a straight segment linked to two masses at its extremities, and which has been improved by an intelligent inversion method using Hopfield (HNN) neurons [13-15]. Our work consists first in modelling the asteroid by an inhomogeneous segment whose density profile is a fourth-order polynomial, then in establishing the analytical expression of the gravitational potential generated by this segment as a function of the density parameters. We then establish the dynamic equations of motion of the probe in the vicinity of the segment. At the end we numerically integrate these equations in order to extract particular orbits for different density shapes.

Dynamic Equations in the Vicinity of the Segment

Consider a segment, of mass M and length $2l$, extending along the axis $(x'x)$ of a reference frame $R(x,y,z)$ whose origin O is the centre of the segment (**FIG.1**). The mass density profile is given by $\lambda(x)=b-ax^2+cx^4$ with a , b and c are positive constants related to the mass of the segment by $M = 2bl - \frac{2}{3}al^3 + \frac{2}{5}cl^5$.

Potential generated by the segment

The potential gravitational per unit mass created by this one dimensional body at a certain point P in the space is given by the line integral:

$$U(P) = -G \int \frac{dm}{r} \tag{1}$$

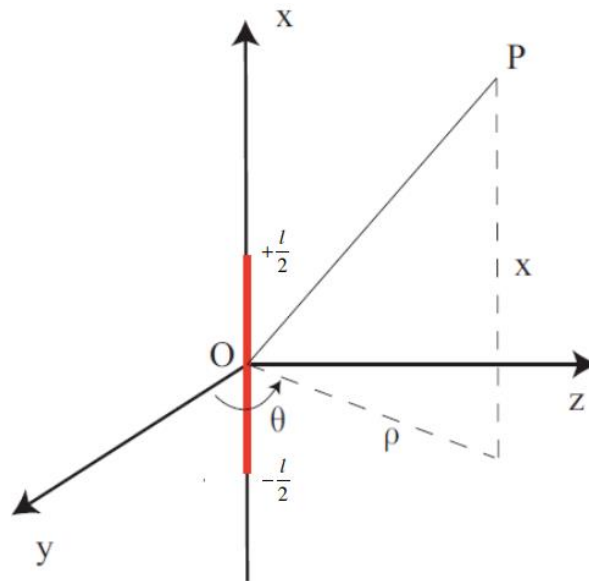


FIG. 1 Study coordinates (ρ, θ, x) .

with G is the gravitational constant and dm is the mass element located at the point H of the segment and of abscissa x_H , as it is represented on **FIG. 2**. We define a new variable of integration $0 \leq v \leq 1$ given by $v = \frac{1}{2} (1 + \frac{x_H}{l})$. The distance r is given by [1]:

$$r^2 = r_1^2 + 4l^2v^2 + (r_2^2 - r_1^2 - 4l^2)v \tag{2}$$

where r_1 and r_2 are the distances between the point P and the ends of the segment. The mass element becomes:

$$dm = 32cl^5 \left[v^4 - 2v^3 + \left(\frac{5}{4} - \frac{a}{4cl^2} \right) v^2 + \left(\frac{a}{4cl^2} - \frac{1}{4} \right) v + \frac{b - al^2 + cl^4}{16cl^4} \right] dv \tag{3}$$

The equation (3) becomes:

$$U(P) = -G \int_0^l \frac{a_4v^4 + a_3v^3 + a_2v^2 + a_1v + a_0}{\sqrt{v^2 + Bv + C}} dv \tag{4}$$

B and C are functions of the position of point P, they are given by:

$$B = \frac{r_2^2 - r_1^2 - 4l^2}{4l^2} ; C = \frac{r_1^2}{4l^2} \tag{5}$$

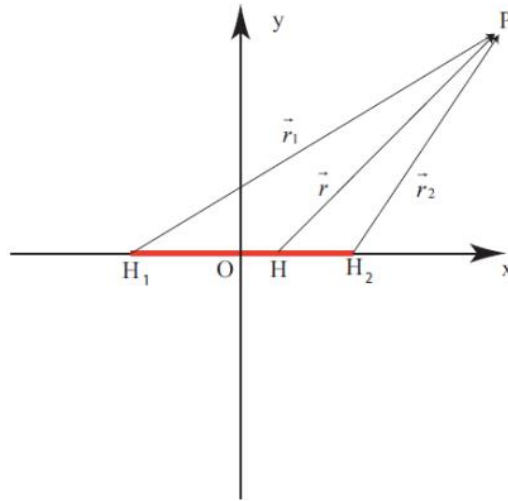


FIG. 2 New coordinates r_1 and r_2 .

a_0, a_1, a_3 and a_4 are the constants given by:

$$a_0 = b - al^2 + cl^4, a_1 = 4l^2(a - cl^2), a_3 = -32cl^4, a_4 = 16cl^2$$

After calculation and simplification of equation (6), we establish the analytical form of the potential generated by this inhomogeneous segment:

$$U(P) = -G \left[z_1 + \frac{r_1}{2l} z_2 + \frac{r_2}{2l} z_3 + z_4 \operatorname{Ln} \left(\frac{s+2l}{s-2l} \right) \right] \tag{6}$$

The coefficients $(z_i)_{i=1..4}$ are auxiliary functions of the position of point P, their expressions are:

$$z_1 = -\frac{55}{48} a_4 BC^{\frac{3}{2}} + \frac{2}{3} a_3 BC^{\frac{3}{2}}$$

$$z_2 = \frac{35}{64} a_4 B^3 - \frac{5}{8} a_3 B^2 + \frac{3}{4} a_2 B - a_1$$

$$z_3 = -\frac{35}{64} a_4 B^3 + \left(\frac{35}{96} a_4 + \frac{5}{8} a_3 \right) B^2 - \left(\frac{5}{12} a_3 + \frac{7}{24} a_4 + \frac{3}{4} a_2 \right) B + \frac{55}{48} a_4 B C - \left(\frac{3}{8} a_4 + \frac{2}{3} a_3 \right) C + a_1 + \frac{1}{2} a_2 + \frac{1}{3} a_3 + \frac{1}{4} a_4$$

$$z_4 = \frac{35}{128} a_4 B^4 - \frac{5}{16} a_3 B^3 - \frac{15}{16} a_4 C B^2 + \frac{3}{8} a_3 B^2 + \frac{3}{4} C B - \frac{1}{2} a_1 B + \frac{3}{8} a_4 C^2 - \frac{1}{2} a_2 C + a_0$$

The expression (6) represents the gravitational potential generated by an inhomogeneous segment of mass line density given by $\lambda(x)=b-ax^2+cx^4$. The case of a parabolic distribution is obtained by giving a $c = 0$ and the homogeneous one is obtained by giving a $a = c = 0$ [8,1].

Equations of motion

The dynamic study of a test particle, of unit mass, placed at the point P where the gravitational field generated by the inhomogeneous segment prevails, is done in the sidereal reference frame $R(O, x, y, z)$ provided with the cylindrical base as it is represented in **FIG.1**. The Lagrangian of the system is given by $L = \frac{1}{2}(\dot{\rho}^2 + \dot{x}^2 + \rho^2 \dot{\theta}^2) - U(r_1, r_2)$ with $r_1 = \sqrt{\rho^2 + (x+l)^2}$ and $r_2 = \sqrt{\rho^2 + (x-l)^2}$.

The dynamic equations of motion of the test particle are:

$$\left\{ \begin{aligned} \ddot{\rho} &= \rho \dot{\theta}^2 + G \left[-\frac{165}{192} a_4 \rho B \sqrt{C} + \frac{a_3}{2l^2} \rho \sqrt{C} + \frac{z_2}{2l} \frac{\rho}{r_1} + \frac{z_3}{2l} \frac{\rho}{r_2} \right] \\ &+ G \frac{r_2}{2l} \left[\frac{15}{96l^2} a_4 B \rho - \frac{1}{2l^2} \left(\frac{3}{8} a_4 + \frac{2}{3} a_3 \right) \rho \right] \\ &+ G \left[\left(-\frac{15}{32l^2} a_4 \rho B^2 + \frac{3}{8l^2} a_3 \rho B + \frac{3}{8l^2} \rho C - \frac{a_2}{4l^2} \rho \right) \text{Ln} \left(\frac{s+2l}{s-2l} \right) - 4l \frac{z_4 \rho s}{p(s-4l^2)} \right] \end{aligned} \right. \tag{7}$$

$$\left\{ \begin{aligned} & \ddot{x} = +G \left[\frac{55}{24l} a_4 C^{\frac{3}{2}} - \frac{165}{192l^2} B \sqrt{C} + \frac{a_3}{2l^2} C(x+l) + \frac{z_2}{2lr_1} (x+l) \right] \\ & +G \left[\frac{r_1}{2l} \left(-\frac{105}{32l} a_4 B^2 + \frac{5}{2l} a_3 B - \frac{3}{2l} a_2 \right) + \frac{z_3}{2lr_2} (x-l) \right] \\ & G \frac{r_2}{2l} \left[\frac{105}{32l} a_4 B^2 - \frac{4}{l} \left(\frac{35}{96} a_4 + \frac{5}{8} a_3 \right) B + \frac{2}{l} \left(\frac{5}{12} a_3 + \frac{7}{24} a_4 + \frac{3}{4} a_2 \right) \right] \\ & +G \frac{r_1}{2l} \left[-\frac{105}{48} a_4 C + \frac{55}{99l^2} a_4 B(x+l) - \frac{1}{2l^2} \left(\frac{3}{8} a_4 + \frac{2}{3a_3} (x+l) \right) \right] \\ & -4Gl \frac{xs - ld}{p(s^2 - 4l^2)} z_4 \\ & +G \left[\frac{70}{32l} a_4 B^3 + \frac{15}{8l} a_3 B^2 + \frac{15}{4} BC - \frac{15}{32l^2} a_4 (x+l) B^2 - \frac{3}{2l} a_2 B \right] \text{Ln} \left(\frac{s+2l}{s-2l} \right) \\ & +G \left[\frac{3}{8l^2} (x+l) B - \frac{3}{2} a_3 C + \frac{a_1}{l} + \frac{3}{8l^2} a_4 (x+l) C - \frac{a_2}{4l_2} (x+l) \right] \text{Ln} \left(\frac{s+2l}{s-2l} \right) \end{aligned} \right. \tag{8}$$

$$\ddot{\theta} = -2 \frac{\dot{\rho} \dot{\theta}}{\rho} \tag{9}$$

We obtain the case of a parabolic distribution is obtained by injecting $c=0$ into the equations (7), (8) and (9) [8].

Numerical Examples and Discussions

The resolution of equations (7), (8) and (9) allows describing the dynamic behaviour of the test particle in the area of the inhomogeneous distribution via the coordinates $\rho(t)$, $x(t)$ and $\theta(t)$.

A numerical resolution allows, for different initial conditions, to extract equatorial, meridian and three-dimensional orbits.

Study of resulting orbits

The **FIG. 3** contains the different profiles of the distribution of the matter along the segment. The **FIG.4** to **FIG. 10** contains numerical trajectories in the equatorial plane which is orthogonal to the segment for different initial conditions $[\rho_0, \dot{\rho}_0, x_0, \dot{x}_0, \theta_0, \dot{\theta}_0]$.

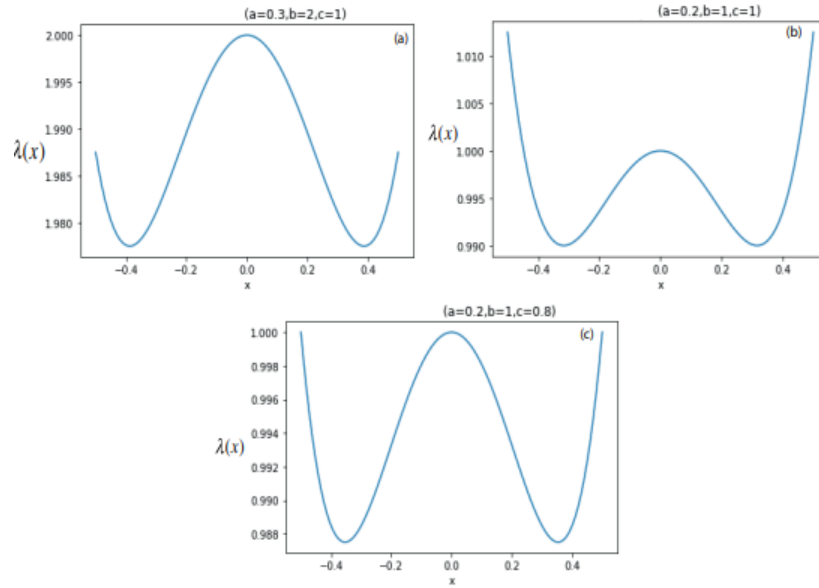


FIG. 3 Profile of density $\lambda(x)=b-ax^2+cx^4$.

Discussion

We are interested in orbits in the (yOz) plane by fixing $x=0$ and $\dot{x} = 0$. In this case the motion variables are $\rho, \dot{\rho}, \theta$ and $\dot{\theta}$.

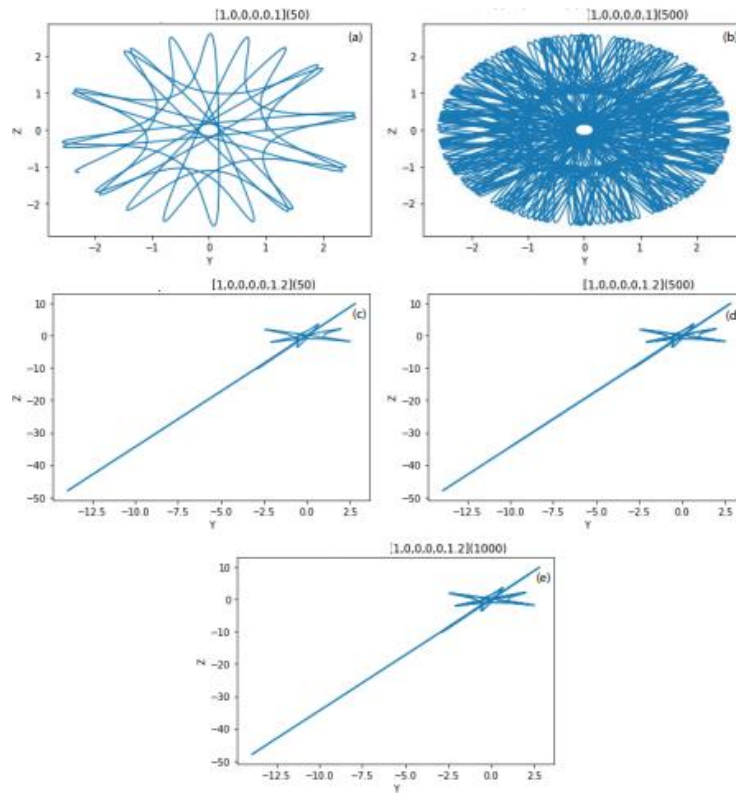


FIG. 4 Profile of density $\lambda(x)=2-0.3x^2+x^4$

For a density $\lambda(x)=2-0.3x^2+x^4$, (FIG.3a):

- We launch the particle with the following initial conditions $\rho = 1, \dot{\rho} = 0, x = 0, \dot{x} = 0, \theta = 0$ and $\dot{\theta} = 0$. The **FIG.4a** shows that for a time of $t=50$ the test particle gravitates around the segment with a precession. The **FIG. 4b** shows that for a time of $t=500$ the precession continues giving a confined orbit between two circles. ^
- The figures **FIG.4a, FIG.4c, FIG.4d** and **FIG.4e** show that when we increase the energy of the particle it remains bound to the segment.

For a density $\lambda(x)=1-0.2x^2+x^4$, (FIG. 3b):

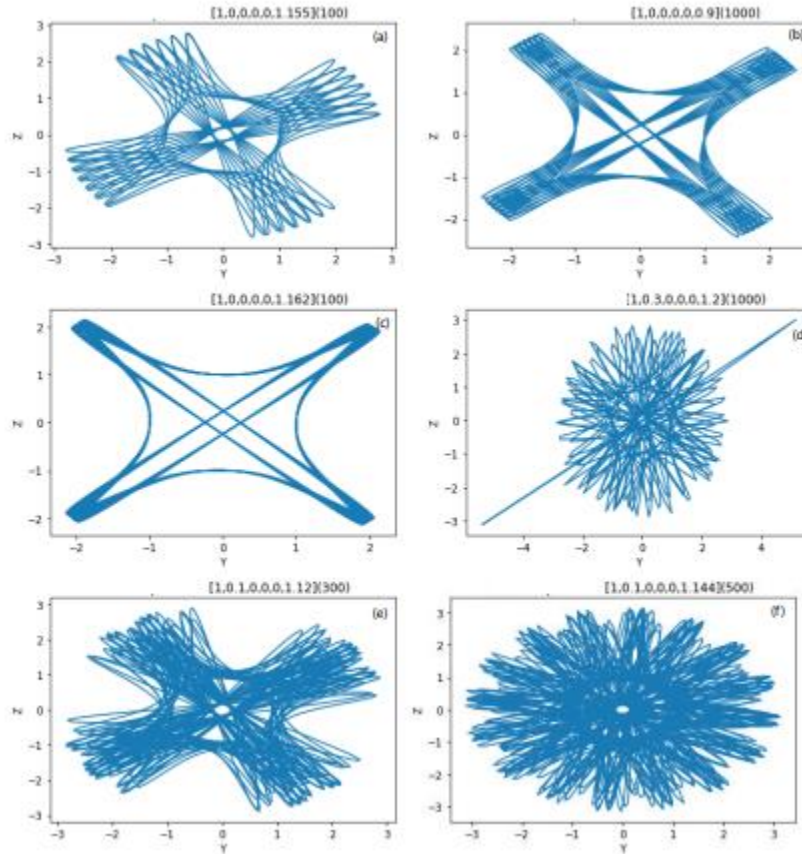


FIG. 5 Profile of density $\lambda(x)=2-0.3x^2+x^4$.

- We launch the particle with the following initial conditions $\rho = 1, \dot{\rho} = 0, x = 0, \dot{x} = 0, \theta = 0$ and $\dot{\theta} = 0.01$. The figures **FIG.7a, FIG. 7b, FIG. 7c** and **FIG. 7d** are obtained by increasing the integration time; they show the existence of a very slow precession giving a confinement state. The **FIG.7e** is obtained by changing the value of $\dot{\theta} = 0.18$. ^
- The orbits which are in the **FIG. 8** are obtained for different initial conditions.

For a density $\lambda(x)=1-0.2x^2+0.8x^4$, (FIG. 3c):

- We launch the particle with the following initial conditions $\rho = 1, \dot{\rho} = 0, x = 0, \dot{x} = 0, \theta = 0$ and $\dot{\theta} = 0.9$. The orbits obtained in **FIG. 9** present other types of resonances.

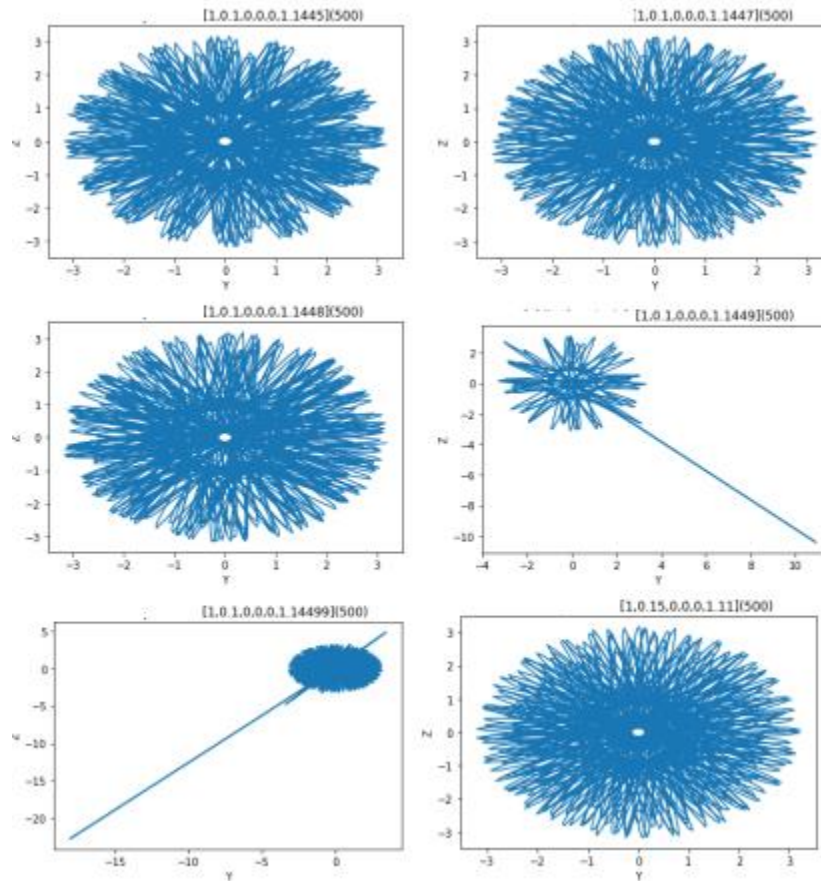


FIG. 6 Profile of density $\lambda(x)=2-0.3x^2+x^4$

- The orbits in FIG. 9 and FIG. 10 are obtained for different initial conditions.

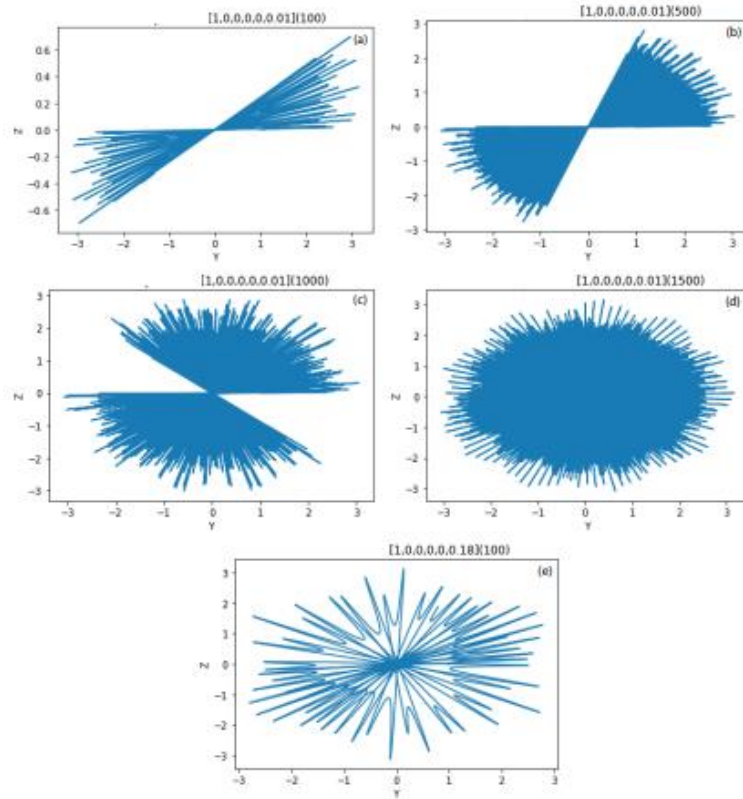


FIG. 7 Model $\lambda(x)=1-0.2x^2+x^4$

Conclusion

In this work, a geo-cruiser has been modelled by a non-homogeneous static segment whose mass density is $\lambda(x)=b-a \times x^2+c \times x^4$ where a , b and c are coefficients modelling the internal structure of the asteroid. After having established the analytical expression of the gravitational potential generated by this mass distribution we established the equations of motion of the probe in the vicinity of this segment. The numerical resolution of these equations showed the existence of confined orbits for well-defined initial conditions allowing the probe to gravitate indefinitely. Among our perspectives we will treat the case where the segment is uniformly rotated around its major axis of inertia in order to search, in the synodic reference frame, for the existence of equilibrium positions and to study their stability as a function of the parameters a , b and c . Using Poincaré’s sections, we will compare the results of our model and that of concerning the chaotic behavior of orbits and the existence of possible bifurcations [9].

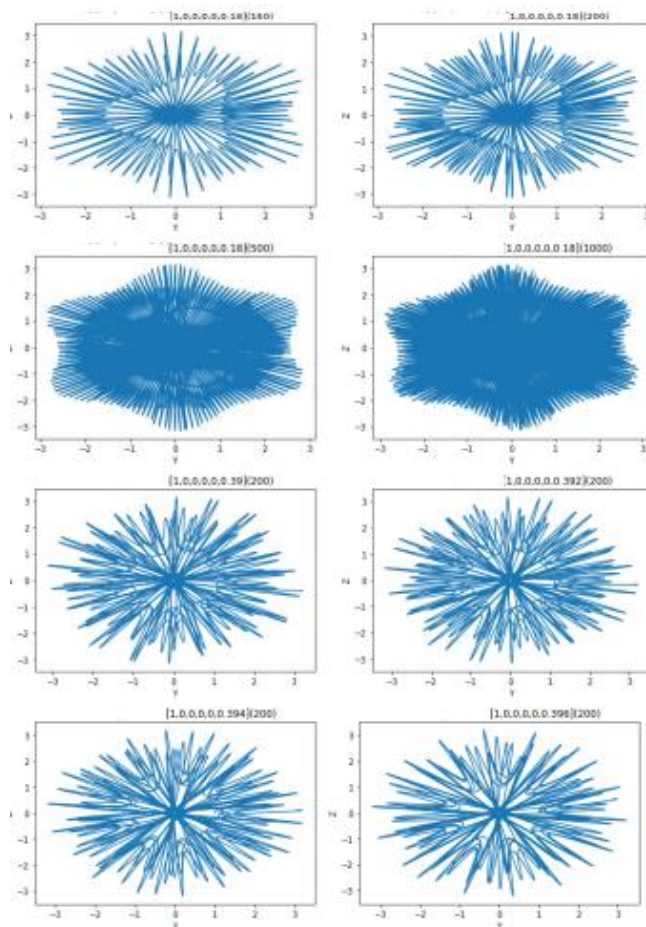


FIG. 8 Model $\lambda(x)=1-0.2x^2+x^4$

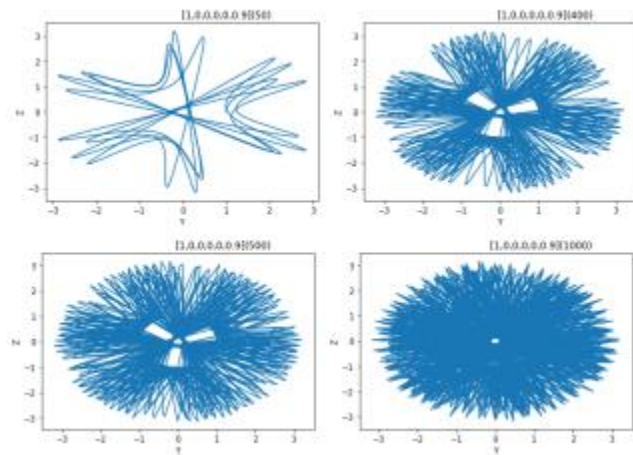


Fig. 9 Model $\lambda(x)=1-0.2x^2+0.8x^4$

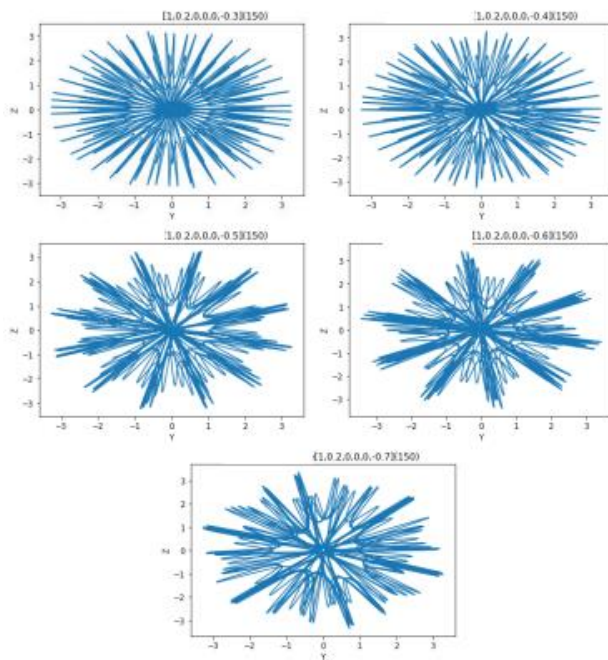


Fig. 10 Model $\lambda(x)=1-0.2 \times x^2+0.8 \times x^4$

REFERENCES

1. Riaguas A, Elipe A, Lara M. Periodic orbits around a massive straight segment. *Celest. Mech. Dyn. Astron.* 1999;73(1-4):169-78.
2. Elipe A, Lara M. A simple model for the chaotic motion around (433) Eros. *J. astronaut. sci.* 2003;51:391-404.
3. Elipe A, Lara M. A simple model for the chaotic motion around (433) Eros. *Adv. Astronaut. Sci.* 2004;116:1-5.
4. Werner RA. The gravitational potential of a homogeneous polyhedron or don't cut corners. *Celest. Mech. Dyn. Astron.* 1994;59:253-78.
5. Werner RA, Scheeres DJ. Exterior gravitation of a polyhedron derived and compared with harmonic and mascon gravitation representations of asteroid 4769 Castalia. *Celest. Mech. Dyn. Astron.* 1996;65:313-44.
6. Bartczak P, Breiter S. Double material segment as the model of irregular bodies. *Celest. Mech. Dyn. Astron.* 2003;86(2):131-41.
7. Bartczak P, Breiter S, Jusiel P. Ellipsoids, material points and material segments. *Celest. Mech. Dyn. Astron.* 2006;96:31-48.
8. Najid NE, Zegoumou M. Potential generated by a massive inhomogeneous straight segment. *Res. Astron. Astrophys.* 2011;11(3):345.
9. Najid NE, El Elourabi H. Equilibria and stability around a straight rotating segment with a parabolic profile of mass density. *Open Astron. J.* 2012;5(1).
10. Najid NE, Zegoumou M, El Elourabi H. Dynamical behavior in the vicinity of a circular anisotropic ring. *Open Astron. J.* 2012;5(1).

11. Romanov VA, Doedel EJ. Periodic orbits associated with the libration points of the homogeneous rotating gravitating triaxial ellipsoid. *Int. J. Bifurc. Chaos.* 2012;22(10):1230035.
12. Romanov VA, Doedel EJ. Periodic orbits associated with the libration points of the massive rotating straight segment. *Int. J. Bifurc. Chaos.* 2014;24(04):1430012.
13. Zeng X, Zhang Y, Yu Y, et al. The dipole segment model for axisymmetrical elongated asteroids. *Astron. J.* 2018;155(2):85.
14. Elipe A, Abad A, Ferreira AF. Dynamics of the Dipole-Segment with Equal Masses and Arbitrary Rotation. In *Recent Trends Chaotic Nonlinear Complex Dyn.* 2022:79-98.
15. Zhao Y, Yang H, Li S, et al. On-board modeling of gravity fields of elongated asteroids using Hopfield neural networks. *Astrodynamic.* 2023;7(1):101-14.